Lunar fast neutron leakage flux calculation and its elemental abundance dependence

O. Gasnault and C. d'Uston
Centre d'Etude Spatiale des Rayonnements, Toulouse, France
W. C. Feldman
Los Alamos National Laboratory, Los Alamos, New Mexico
S. Maurice
Observatoire Midi-Pyrénées, Toulouse, France

Abstract. A numerical code has been developed to simulate fast neutron leakage flux from planetary surfaces. These neutrons are produced in copious number by interactions between galactic cosmic rays and the nuclei of surface material. Their leakage flux spectrum depends on the composition of the upper layers of planetary bodies. Measurement of these neutrons allows the mapping of major compositional units. This technique is successfully used on Lunar Prospector data to obtain global geochemical maps of the lunar surface. With the help of simulations, relations between soil composition and neutron fluxes in the fast energy range [500 keV, 10 MeV] are established. The numerical code reproduces correctly the measurements of fast neutrons over the Moon. Variation in the neutron flux between highland and mare soils is calculated. A simple formula is suggested to estimate quickly the integrated fast neutron leakage flux for a given soil composition.

1. Introduction

Orbital geochemical measurements provide a major contribution to understanding the outer surface layers of a planet. In the case of the Moon, returned samples and in situ analyses have given the landing site compositions with a high accuracy, but this is probably not representative of the entire Moon, particularly for highlands. A more general view was obtained by the acquisition of orbital data during the Apollo missions, but these data were restricted to an equatorial band. Clementine [*Nozette et al.*, 1994] and, more recently, Lunar Prospector [*Binder*, 1998] obtained global mineralogical and geochemical data over the entire lunar surface.

Several methods allow surface investigation from space. Each of them gives complementary results in terms of spatial resolution and geological information. Before the start of space exploration, *Lingenfelter et al.* [1961] suggested use of the neutron leakage flux from planetary surfaces to obtain their compositions. These neutrons are produced in copious numbers by interactions between galactic cosmic rays (GCRs) and the nuclei of surface material. After production (most with energies above a few MeV), neutrons exchange energy with regolith material and eventually come to equilibrium [*Feldman et al.*, 1993b]. The resultant neutron spectrum depends on the composition of the upper surface layer of ~300 g cm^{-2} thickness [*Drake et al.*, 1988]. This technique has been successfully implemented aboard Lunar Prospector [*Feldman et al.*, 1998a] and will soon be on Mars Surveyor 2001 [*Boynton et al.*, 1999]. That provides global maps of major compositional units, and thereby it helps identify and delineate basaltic from feldspathic units as well as determine the abundance of water in the near-surface regolith [*Reedy*, 1987a].

Physical processes involved in shaping the neutron spectrum are sufficiently well known to numerically simulate the flux spectrum of neutrons that leak from planetary surfaces. We use these simulations here to explore the geochemical information content of fast neutron flux measurements. Previous such studies were carried out for thermal and epithermal observations on the Moon [*Lingenfelter et al.*, 1972; *Feldman et al.*, 1991], Mars [*Feldman et al.*, 1993a; *Drake et al.*, 1994] and Mercury [*Feldman et al.*, 1997]. We use the Geometry and Tracking (GEANT) code library in the present study to develop relations between soil composition and spectrum shapes and integrated fluxes in the fast energy range [500 keV, 10 MeV]. We then apply our results to the Moon by interpreting Lunar Prospector data. An identical set of simulations could be done for Mars, Mercury, meteorites, or comets.

2. Soil and Flux Modeling

Geometry and Tracking (GEANT) is a system of numerical codes designed to simulate high-energy processes within any experimental setup; it is provided by the European Organization for Nuclear Research (CERN, Geneva, Switzerland) [*Brun et al.*, 1994]. GEANT is designed to model complex three-dimensional (3 D) detectors, and its energy range is broad, ranging from meV to GeV with GCALOR interface [*Zeitnitz and Gabriel*, 1996]. The GEANT program, based on Monte Carlo methods, simulates the passage of elementary particles and photons, the production of secondaries, and their transport through matter. GEANT evaluates the probability of occurrence of each physical process and generates the final state after interaction. The processes currently implemented are hadronic interactions, electromagnetic processes, muonic interactions, ionization by charged particles, and multiple scattering. The setup where the particles are transported is represented by a structure of geometrical volumes defined by the user. The user defines the matter that fills each volume according to its nature, which can be either predefined (vacuum, natural iron, etc.) or

specified by its atomic number, atomic weight, density, and so on. About a hundred kinds of particles could be simulated (gamma, neutrons, protons, etc.). The user's computer code records the position, the direction, the creation of particles, or the energy deposition at tracking time.

A dedicated code was written to use this powerful calculation tool to improve the interpretation of the leakage fast neutron measurements in orbit above the Moon. This code consists of a lunar soil model and of a GCR irradiation model; neutron processes in the surface are calculated, and the leakage flux spectrum is estimated. The results are presented and discussed in this paper.

The planet surface is modeled as a cylinder that is large and dense enough to contain all secondaries, without losses (1200 cm in diameter, 1200 cm in height, and a density of 3 g cm^{-3}). The upper surface of the cylinder represents the lunar surface, and the height of the cylinder is the thickness of the surface layer. Galactic cosmic rays are injected onto a little disk at the surface center. This irradiation is isotropic over 2π sr, made of protons with a *Castagnoli and Lal* [1980] energy spectrum (see correction of *Reedy* [1987b]) taken for an average solar activity (Figure 1). The amplitude of this spectrum is multiplied by a factor 1.4 to take GCR alpha particles into account [*Masarik and Reedy*, 1994]. Highlands represent more than 80% of the lunar surface; therefore the first soil composition is chosen to be one of ferroan anorthosite (FAN), which is a major constituent of regolith in these terrains. Indeed, *Davis and Spudis* [1985, 1987] suggested that the composition of the highland crust observed by Apollo 15 and 16 can be modeled by a mixture of about 65-68% FAN, 25-29% mare basalt, and 3-10% KREEP-troctolite-norite [*Davis and Spudis*, 1985, 1987]. The FAN composition that we used is shown in Table 1 and is the same as that used by *Metzger and Drake* [1990] and *Feldman et al.* [1991]; it was derived from the LGO Science Workshop report [*Phillips*, 1986]. From this soil, several compositions have been constructed by changing the abundance of one oxide at the expense of all others.

We simulate the fast neutron leakage fluxes from these soils and study the compositional variation effects on the flux. Here the (differential) leakage flux is defined as

$$\Phi = \frac{N_{\mathrm{fnc}}}{S_{\mathrm{ip}} T_{\mathrm{si}} \Delta E},$$

where N_{fnc} is the number of neutrons crossing the top disk of the soil cylinder (1200 cm in diameter) (this number is given as the result of the simulations); S_{ip} is the surface of the irradiated area (2 cm in diameter); T_{si} is the time of GCR irradiation; and ΔE is the energy bin width. T_{si} is calculated according to the relationship that gives the flux of an isotropic emission through a planar surface [*Rybicki and Lightman*, 1979]:

$$T_{\mathrm{si}} = \frac{N_{\mathrm{i}}}{S_{\mathrm{ip}} \varphi_{\mathrm{GCR}} \pi},$$

where N_i is the number of incident simulated particles and φ_{GCR} is the GCR flux in space (0.323 particle cm^{-2} s^{-1} sr^{-1} in our simulations). Between 20,000 and 50,000 incident particles were used per simulation in this work.

The planet surface is assumed to be uniform, so the previous flux is independent of the source position at the surface. With this assumption, the total escaping flux due to 1 cm^2 irradiation is equivalent to the leakage flux from 1 cm^2 of surface when the whole planet surface is irradiated. The total flux for the entire planetary surface is then equal to the previous one (local flux integrated over the surface and divided by this surface). In the remainder of this paper, this local flux is called Φ (neutron cm^{-2} s^{-1} MeV^{-1}). In a second part of this work, the integrated flux between 500 keV and 8 MeV, $J=\int\Phi\, dE$ (neutron cm^{-2} s^{-1}), will be calculated. The abundance of an atom X, in weight fraction, will be written [X].

3. Results and Discussion

Following their production at high energies (MeV), neutrons moderate in surrounding material by random nonelastic and elastic collisions with the nuclei of the lunar soil. Neutrons lose energy at each collision, until they escape or are captured; the energy transfer from neutrons to nuclei is maximized through collisions with nuclei of lower atomic weight (oxygen in lunar soils), especially through elastic collisions at the lower energies. The resultant leakage energy spectrum is strongly weighted toward lower energies compared with the production spectrum. The fast part of the spectrum reflects a balance between the production and energy-loss rate due to collisions. Our results explore the factors that influence the fast part of the energy spectrum.

3.1. Lunar Fast Neutron Leakage Flux

The first result of this work is the calculation of the neutron leakage flux between 500 keV and 10 MeV from a uniform surface that has a FAN composition (Figure 2). Its general shape is consistent with previous estimations [*Lingenfelter et al.*, 1961; *Armstrong and Alsmiller*, 1971]. Beyond 3 MeV this neutron leakage flux spectrum can be approximated as a power law ($0.74\times E^{-1.5}$); below 3 MeV several features are superimposed to the power law: there is a peak at 2.4 MeV and several resonance lines between 1 and 2 MeV. The total cross section of reaction between neutron and oxygen atom is also shown in Figure 2. It is seen to be a dominant factor in shaping the Φ spectrum. In particular, it shows the association of resonance peak in the cross section with minimal intensity in the equilibrium neutron flux spectrum. This result is not surprising because oxygen is the most abundant element in lunar soil (~0.45 in weight fraction). These resonances are not useful for determining soil composition because [O] does not vary

significantly on the Moon. However, the overall intensity of fast neutrons is important because some atoms like Fe and Ti increase the amplitude of the spectrum sufficiently to be measured from an orbiting spacecraft. Figure 3 shows two calculated neutron spectra, one from a lunar soil with no Fe and the other with 30% Fe; these spectra are presented with Lunar Prospector energy binning. Inspection shows that Fe significantly increases the amplitude of the fast neutrons.

This amplitude is also a function of solar activity. GCR irradiations of Figure 1 for quiet Sun conditions (highest irradiation, φ_{GCR}=0.437 particle cm^{-2} s^{-1} sr^{-1}) and for active Sun conditions (lowest irradiation, φ_{CGR}=0.172 particle cm^{-2} s^{-1} sr^{-1}) have been simulated. Although the GCR flux is 2.5 times higher for a quiet Sun than for an active Sun, this variation takes place at lowest energies, and neutrons are basically produced in greater number by the highest-energy protons. This fact explains why the calculated amplitude of the fast neutron flux is only 1.9 times higher for a quiet Sun than for an active Sun. It should also be noted that the neutron flux energy spectrum does not depend on solar activity, as was already demonstrated by *Armstrong and Alsmiller* [1971] and *Drake et al.* [1988].

A comparison between the simulated neutron spectrum and the measured lunar spectrum is presented in Figure 4. Here the simulated spectrum is calculated for an average GCR spectrum incident on a pure FAN soil. The measured spectrum corresponds to the summed data acquired during 20 consecutive 2-week maps cycles (20×14 days) over the entire Moon (see also S. Maurice et al., High-energy neutrons from the Moon, submitted to *Journal of Geophysical Research*, 1999) (hereinafter referred to as submitted manuscript, 1999). Figure 4 shows that the absolute agreement is rather good. Differences below 3 MeV can probably be explained by the actual mixing of soil composition: the FAN approximation is not representative of the average lunar soil. Some differences may also come from use of the average GCR energy spectrum. On the other hand, there are also some experimental uncertainties in the detector efficiency and energy cut off threshold that could explain the differences (Maurice et al., submitted manuscript, 1999).

3.2. Variation in J=∫Φ dE

In an attempt to compare our simulation with observed flux spectra in lunar orbit, we also calculate the flux integrated between 500 keV and 8 MeV (here defined as *J*). The variations in *J* are studied for 41 imaginary compositions constructed by increasing or decreasing the abundance of one oxide at a time in a FAN soil, the other oxide abundances being changed to keep the same proportions between them and a total weight fraction abundance of 1. For example, if the abundance of SiO_2 is assumed to be $[O_{Si}] = 0.3$ instead of 0.442 in the FAN composition, then the abundance [OZ] of the oxide of the element Z (Z ≠ Si) will be $[O_Z] = F\times[O_Z]^{FAN}$, where $[O_Z]^{FAN}$ is the abundance of the oxide of the element Z in the FAN composition (Table 1). *F* is a normalization factor as

$$\sum_Z [O_Z] = 1 \Rightarrow F = \frac{1-[O_{Si}]}{1-[O_{Si}]^{FAN}} = \frac{1-0.3}{1-0.442}.$$

Consequently, if the abundance of one oxide is increased, the abundance of all the other oxides decrease and vice versa. The results of this set of simulation are shown in the seven panels of Figure 5; each one presents the calculated value of J as a function of one of the chemical element concentrations which is linked to the previous oxide abundances by

$$[M_Z] = \frac{A(M_Z)}{A(O_Z)}[O_Z],$$

where $A(M_Z)$ is the atomic mass of the metal Z and $A(O_Z)$ is the atomic mass of the oxide.

The initial value of each chemical element concentration in the FAN composition is indicated in each panel by a vertical line. We note in Figure 5 the linear relationship between *J* and the abundance of each element. These linear dependences reveal several types of behavior: (1) *J* decreases with the abundance of Na, Mg, Si, and Al, (2) the slope of the curve is slightly positive for Ca, and, finally, (3) *J* increases strongly for Fe and Ti. In order to understand these characteristics, two factors must be considered: (1) the neutrons production and (2) their transport through the soil.

Neutron production is illustrated in Figure 6, which shows the energy spectra of the neutrons created in two target materials: FAN and pure iron. These neutrons are produced by spallation and by evaporation from excited nuclei; the neutron distribution of this last process is a Gaussian around a few MeV. For each target material, two spectra are presented that correspond to (1) the neutrons created from direct interaction of primary GCR particles (first generation of secondary particles created by spallation and evaporation) and (2) the total number of created neutrons. As shown in Figure 6, most of the neutrons are not produced directly by the GCR particles but instead are created during the nuclear cascade involving all secondary particles. This fact implies that the distance from the surface to the location of most of the neutron production processes is much larger than the penetration depth of the primary GCR particles. The dimensions of our scattering volume (radius and height of the cylinder) in the calculations were therefore chosen to be larger than this penetration depth. It is shown, moreover, in Figure 6 that most of the created neutrons have energies around 1 MeV and that the resultant neutron spectra display spectral shapes that are practically independent of target composition. On the other hand, some atoms produce more neutrons than others. For example, *Drake et al.* [1988] show that Fe produce more neutrons than Si or O, which produce more neutrons than H. In our simulations we have reproduced such characteristics. In particular, it is demonstrated in close

agreement with *Drake et al.* [1988] that pure iron (and, similarly, titanium) produces more than 2 times the number of neutrons per incident GCR particle than are produced by oxygen and most of the main elements constituting soil compositions. The excess of neutrons in Ti and Fe nuclei (see neutron-proton values in Table 1) may explain at least part of this effect. Actually, a certain fraction of reactions break the struck nucleus apart, forming nuclei of lower mass. Since the valleys of nuclear stability of most of the lower-mass nuclei have equal numbers of neutrons and protons, there will be an excess of neutrons when an iron or titanium is hit and broken down to lower-mass residual nuclei. Thus one of the reasons why the *J* quantity is very dependent on Fe and Ti abundances is that those nuclei are the source of more neutrons than the other elements that have been considered here.

The transport of the created neutrons up to the surface, where they will leak out, will imprint on this created neutron spectrum the effect of the interactions with the medium. This is illustrated in Figure 7, which shows the spectrum of the escaping neutrons in comparison with the created neutron spectrum, both related to the GCR irradiation of 1 cm2 of a FAN soil. As already mentioned in section 3.1, the main characteristic features of the escaping spectrum are related to the neutron-oxygen interaction cross section (see Figure 2). This structure is completely absent for the pure iron escaping spectrum. Consequently, neutron transport in the soil makes the fast neutron leakage spectrum representative of the soil composition. The interactions also have the effect of transferring neutrons from higher energies to lower energies until they escape or reach thermal equilibrium. This effect appears clearly in Figure 7, which shows a difference between produced neutrons and leakage flux, amounting to more than one order of magnitude at 10 MeV, whereas the two spectra approach one another at around 100 keV and cross between 10 and 100 keV. Such an effect reflects the cross section of neutron collisions with surrounding nuclei, making neutrons lose some kinetic energy, but in the 500 keV to 10 MeV energy range the cross sections for reactions of neutrons with all nuclei, except oxygen, are quite similar. Variations in composition should therefore not change the mean cross section of the soil or the time needed to transfer neutrons to epithermal (0.3 eV to 500 keV) energy range. Consequently, the calculated variations of neutron fluxes, when the composition changes, are mainly due to the corresponding neutron production variations rather than cross-section variations (for the elements that have been considered here).

As noticed earlier, the fast neutron leakage flux increases strongly with [Fe] or [Ti] (Figure 5): this variation of *J* appears to be a linear function of the Fe or Ti weight fraction with a variation rate of 1.3 neutron cm^{-2} s^{-1} weight $fraction^{-1}$. Note that the strong effects of Fe and Ti are studied separately by this method because Fe and Ti abundances in FAN are low; furthermore, when one is increased, the other becomes lower. On the Moon [*Metzger and Drake*, 1990] the expected abundance range (in weight fraction) for Fe is roughly from 0.01 in highlands to 0.15 in maria; according to our simulations, this corresponds to a variation in *J* between 1.19 and 1.37 neutron cm^{-2} s^{-1}, that is to say, a 15% variation. Such a kind of significant variation can be measured by a neutron spectrometer aboard a spacecraft orbiting the Moon. Likewise, the calculated flux increase due to [Ti] variations is strong, but the net effect on leakage neutron spectra is not as great as that for [Fe]: from 0 to 0.013 in highlands up to 0.078 in maria. The associated integral flux range should be correspondingly low but still significant: from 1.18 to 1.27 neutron cm^{-2} s^{-1}, that is to say, 8%.

As the variations of *J* with weight fractions seem to be linear, the slopes of these variations are a function of the atomic abundances. Thus these slopes should be representative of each type of atom contribution in the flux spectra. However, the above variation rate of *J* with [Fe] and [Ti], of about 1.3 neutron cm^{-2} s^{-1} weight $fraction^{-1}$, is underestimated because the effect of the other atoms is not negligible: the trends in Figure 5 are produced by the variation of abundance of all the elements which have an oxide. Actually, when [Na], [Mg], [Al], or [Si] increases, there is a corresponding decrease of [Fe] and [Ti] in the composition which contributes mainly to decrease in *J* with the above rate. To get the correct values of the variation rate of *J*, all the variations in the composition must be taken into account simultaneously.

Let us suppose the abundance variations in this simulation set are sufficiently small to have a linear effect on *J*. Besides, when *J* is plotted versus abundance of one type of atom as in Figure 5, the calculated points are roughly aligned for all considered values of the abundance of any atom present in FAN composition as given in Table 1. Then it is possible to calculate *J* using a linear combination of the eight atom abundances that make the soil composition. From our 41 soil compositions derived from FAN, there is an overdetermined system of linear equations linking abundance of each atom with the integrated value of the flux. A coefficient α_X was assigned to each atom abundance and is estimated by orthogonally projecting onto subspaces, using the Singular Value Decomposition (SVDC) procedure in Interactive Data Language (IDL, Research Systems, Inc.). In this way, eight coherent coefficients α_X (Table 2) were found; then *J* can be calculated as ${}_X\Sigma(\alpha_X \times [X])$. "Coherent" means that all the plots like Figure 5 are well reproduced by this formula with a correlation factor between 0.752 and 0.998. These coefficients indicate the impact of each type of atom in the total integrated value: the higher the α_X coefficient, the more sensitive to [*X*] variations. Table 2 indicates again the importance of [Ti] and [Fe] variations with an associated variation rate of *J* of about ~2.8-3.0 neutron cm^{-2} s^{-1} weight $fraction^{-1}$. This value is higher than the first estimate in this work and takes into account the presence of the eight atoms in the composition. Fur-

thermore, with coefficients between 1.3 and 2.3 neutron cm^{-2} s^{-1} weight $fraction^{-1}$, Si, Al, Ca, Mg, and Na have a nonnegligible part in the calculation of *J*; of course, O is not negligible either; its low coefficient is balanced by its high abundance. Also, α_{Na} α_{Mg} α_{Al}, and α_{Si} are positive even if the trend in Figure 5 for these elements is negative. This is explained by the fact that the increase of the flux with [Na], [Mg], [Al], or [Si] is lesser than the decrease due to the reduction of all other abundances.

In order to check the validity of the above α_X coefficients on *J*, another set of simulations was made using several typical lunar rock compositions (Table 3 [*Metzger and Drake*, 1990; *Feldman et al.*, 1991] derived from the LGO Science Workshop report [*Philipps*, 1986]). The *J* values that have been obtained are presented in Figure 8 as a function of the corresponding Fe abundance in Figure 8a and of the corresponding Ti abundance in Figure 8b. A strong linear dependence on [Fe] is clearly shown. This trend over various terrains proves the dominant effect of [Fe] that is never <3.8% in all these soil types. With the Apollo 11 and Apollo 17 soils, the Ti enrichment may well explain the slight excess of *J* relative to the linear [Fe] dependence (dotted line) determined in Figure 5. When looking at Figure 8b, where *J* values have been plotted as a function of [Ti], there seems to be a much larger dependence of *J* relative to titanium concentration (dashed line) than in the modified FAN soil (dotted line). This is because these rocks have Fe and Ti abundances that increase together, while in the modified FAN soils the Fe and Ti concentrations change in opposition. It must also be noted that these rocks are made of some additional elements (S, K, Cr, and Mn) which may have concentrations that exceed [Ti]. Because these soils cannot be deduced from the FAN composition, they will constitute a test of the validity of the $J=_X\Sigma\alpha_X[X]$ formula.

The above linear equation was applied to the case of these typical lunar rocks. As there was no S, K, Cr, or Mn in the FAN soils, α_X coefficients for these elements have not been determined and are taken equal to 0; this means that the effect of these elements is ignored. Comparison between these calculated values and the values of *J* given by the full simulation is shown in Figure 9. The agreement between the two results is very good with a correlation factor of 0.997. The ignored contributions of S, K, Cr, and Mn could be neglected because these elements represent a very small fraction (less than or around 1% in total) of the composition. This agreement suggests that our derived α_X coefficients can be used to estimate the integrated fast neutron flux from any ordinary dry planetary soil.

The integrated flux that is measured aboard an orbiting spacecraft results from the mixing of soils within the detector surface space resolution. However, as shown by the above studies, variations in *J* are due mostly to the strong effect [Ti] or [Fe], and thus this integral parameter is a good criterion to discriminate between highlands soils, which are poor in Ti or Fe, and the maria, which contain larger amounts of iron.

4. Conclusion

In order to help interpret the Neutron Spectrometer observations made aboard Lunar Prospector, the formation of the fast neutron spectrum has been examined. For this purpose, a numerical code based on the GEANT library has been developed to simulate the creation and the transport of neutrons in planetary surfaces exposed to galactic cosmic rays. The main points of this work are as follows:

1. It makes a dedicated study of the characteristics of the leakage of fast neutrons from a planetary surface.
2. Our numerical code procedure yields a fast neutron energy spectrum that is in agreement with previous simulations [*Drake et al.*, 1988].
3. The simulated energy spectrum of the fast neutrons escaping from a typical lunar highland rock is found to be in quantitative agreement with the spectrum measured by the Lunar Prospector Neutron Spectrometer over the entire Moon.
4. The spectral features of the leaking fast neutrons contain only marginal information on the chemical composition of the soil components. The spectra are mainly marked by the shape of the interaction cross section of neutron with oxygen since this atom makes more than 40% of the soil composition in all cases.
5. The integral flux of neutrons from 0.5 to 8 MeV shows a significant dependence on the abundances of Fe and Ti. Since iron is a known marker of mare rocks (of which it always constitutes more than 10% per weight), the present work demonstrates the ability to distinguish between maria and highlands using the measured integral flux of fast neutrons.
6. An easy method for a rapid estimate of this fast neutron flux as a function of the soil composition is proposed. It consists of a linear combination of the abundances of the major elements with a set of coefficients associated with each element.

Use of these coefficients should allow a determination of the Fe and Ti composition using fast neutron and other related observations made aboard the Lunar Prospector mission and also later at Mars aboard the Mars Surveyor 2001 mission. We plan an extension of the present work to include the presence of hydrogen in the soil in order to provide constraints on the depth of burial of enhanced hydrogen abundances found in polar lunar terranes [*Feldman et al.*, 1998b].

Acknowledgments. The authors would like to thank the referees, one of whom is L. Haskin and one of whom remains anonymous, for their useful comments.

References

Armstrong, T.W., and R.G. Alsmiller Jr., Proc. of the Lunar Sci. Conf., *2nd*, 1971.

Binder, A.B., Lunar Prospector: Overview, *Science, 281*, 1475-1476, 1998.

Boynton, W.C., et al., Scientific investigation of the elemental composition of Mars by means of the Mars Surveyor 2001 gamma-ray spectrometer, paper presented at Mars Exploration Program & Sample Return Missions Symposium, Cent. Natl. d'Etude Spatiales, Paris, 1999.

Brun, R., F. Carminati, and S. Giani, GEANT detector description and simulation tool, *Program Library Long Writeup W5013*, Eur. Organ. For Nucl.Res., Geneva, 1994.

Castagnoli, G., and D. Lal, Solar modulation effects in terrestrial production of carbon 14, *Radiocarbon, 22*, 133-158, 1980.

Davis, P.A., and P.D. Spudis, Petrologic province maps of the Lunar highlands derived from orbital geochemical data, *Proc. Lunar Planet. Sci. Conf. 16th*, Part 1, *J. Geophys. Res., 90*, suppl., D61-D74, 1985.

Davis, P.A., and P.D. Spudis, Global petrologic variations on the Moon : A ternary-diagram approach, *Proc. Lunar Planet. Sci. Conf. 17th*, Part 2, *J. Geophys. Res., 92*, suppl., E387-E395, 1987.

Drake, D.M., W.C. Feldman, and B.M. Jakosky, Martian neutron leakage spectra, *J. Geophys. Res., 93*, 6353-6368, 1988.

Drake, D.M., M. Drosg, R.C. Byrd, R.C. Reedy, D.A. Clark, P.A.J. Englert, J.F. Dempsey, S.G. Bobias, and L. Harris, Experimental and numerical simulation of Martian neutron distribution, *Nucl. Instrum. Methods Phys. Res. Sect. B, 84*, 337-356, 1994.

Feldman, W.C., R.C. Reedy, and D.S. McKay, Lunar neutron leakage fluxes as a function of composition and hydrogen content, *Geophys. Res. Let., 18*, 2157-2160, 1991.

Feldman, W.C., W.V. Boynton, B.M. Jakosky, and M.T. Mellon, Redistribution of subsurface neutrons caused by ground ice on Mars, *J. Geophys. Res., 98*, 20855-20870, 1993a.

Feldman, W.C., W.V. Boynton, and D.M. Drake, Planetary neutron spectroscopy from orbit, in *Remote Geochemical Analysis: Elemental and Mineralogical Composition*, edited by C.M. Pieters and P.J. Englert, pp. 213-234, Cambridge Univ. Press, New York, 1993b.

Feldman, W.C., B.L. Barraclough, C.J. Hansen and A.L. Spague, The neutron signature of Mercury's volatile polar deposits, *J. Geophys. Res., 102*, 25,565-25,574, 1997.

Feldman, W.C., B.L. Barraclough, S. Maurice, R.C. Elphic, D.J. Lawrence, D.R. Thomsen, and A.B. Binder, Major compositional units of the Moon: Lunar Prospector thermal and fast neutrons, *Science, 281*, 1489-1493, 1998a.

Feldman, W.C., S. Maurice, A.B. Binder, B.L. Barraclough, R.C. Elphic, and D.J. Lawrence, Fluxes of fast and epithermal neutrons from Lunar Prospector: Evidence of water ice at the lunar poles, *Science, 281*, 1496-1500, 1998b.

Lingenfelter, R.E., E.H. Canfield and W.N. Hess, The Lunar neutron flux, *J. Geophys. Res., 66*, 2665-2671, 1961.

Lingenfelter, R.E., E.H. Canfield, and V.E. Hampel, The Lunar neutron flux revisited, *Earth Planet. Sci. Let., 16*, 355-369, 1972.

Masarik, J., and R.C. Reedy, Effects of bulk composition on nuclide production processes in meteorites, *Geochim. Cosmochim. Acta, 58*, 5307-5317, 1994.

Metzger, A.E., and D.M. Drake, Identification of lunar rock types and search for polar ice by gamma-ray spectroscopy, *J. Geophys. Res., 95*, 449-460, 1990.

Nozette S., et al., The Clementine mission to the Moon: Scientific overview, *Science, 266*, 1835-1839, 1994.

Phillips, R. (Ed.), Contributions of a Lunar Geoscience Observer Mission to fundamental questions in lunar science, in *LGO Science Workshop*, Dep. of Geol. Sci., Southern Methodist Univ., Dallas, Tex., 1986.

Reedy, R.C., Gamma-ray and neutron spectroscopy of planetary surfaces and atmospheres, *AIP Conf. Proc., 170*, 1987a.

Reedy, R.C., Nuclide production by primary cosmic-ray protons, *Proc. Lunar Planet. Sci. Conf. 17th*, Part 2, *J. Geophys. Res., 92*, suppl., E697-E702, 1987b.

Rybicki, G.B., and A.P. Lightman, Fundamentals of radiative transfer, in *Radiative Processes in Astrophysics*, J. Wiley, New York, 1979.

Zeitnitz, C., and T.A. Gabriel, *The GEANT-CALOR Interface User's Guide*, Oak Ridge Nat. Lab., Tennessee, 1996.

Figure 1. Galactic cosmic ray (GCR) spectrum for a quiet and an active Sun [*Castagnoli and Lal*, 1980; *Reedy*, 1987b; *Masarik and Reedy*, 1994]. The bold curve is the averaged GCR flux on a solar cycle used in the simulations. The plotted flux is normalized by steradian and multiplied by a factor of 1.4 to take GCR alpha particles into account.

Figure 2. Bold curve: fast neutron leakage flux from uniform lunar soil of ferroan anorthosite (FAN) simulated between 500 keV and 10 MeV. Dotted curve: power law fit of the flux between 3 MeV and 10 MeV. Thin curve: total cross section of the oxygen-neutron interactions (ENDF/B-VI library).

Figure 3. Illustration of the Fe effect on the general shape of the simulated lunar neutron leakage flux. Energy bands correspond with Lunar Prospector fast neutron spectrometer ones. The bold curve represents the case without Fe. The thin curve is the case with 30% of Fe in the soil (in weight).

Figure 4. Spectrum of fast neutron leakage flux measured by Lunar Prospector over the Moon (Maurice et al., submitted manuscript, 1999). Asterisks represent the flux simulated for a soil of FAN and an averaged solar activity (this work).

Figure 5. Variation in integrated (500 keV to 8 MeV) value of fast neutron leakage flux from a soil of FAN with the abundance (weight percent) of Na, Mg, Al, Si, Ca, Ti, and Fe. Asterisks are simulation results ; the lines are linear fits. In each panel the initial composition of FAN is indicated by a vertical line.

Figure 6. Initial energy spectra of the produced neutrons per GCR particle in a FAN soil (solid curves) and in a pure iron soil (dashed curves). The thin curves represent the neutrons directly produced by primary GCR particles (i). The bold curves correspond to the total number of created neutrons (ii). Values are normalized by MeV.

Figure 7. Neutron leakage flux spectrum from a FAN soil compared to the total neutron production in the soil between 10 keV and 10 MeV. The leakage spectrum represents the number of neutrons per second and per MeV leaking out when 1 cm^2 of the surface is irradiated by an averaged GCR flux. The production spectrum represents the number of neutrons created in the soil per second and per MeV when 1 cm^2 of the surface is irradiated by an average GCR flux.

Figure 8. Variation of the simulated integrated values of fast neutron leakage flux for typical lunar rocks (triangles), (see Table 3) relative to their abundance of Fe and Ti. In Figure8b the dashed line is a linear fit for typical lunar rocks. For comparison, the dotted lines represent the linear best fit of the relationship defined in Figure 5 for the modified FAN compositions.

Figure 9. Comparison of the integrated fluxes of fast neutrons as determined by the full numerical simulation (triangles) with the equivalent values calculated using the expression $J={}_X\Sigma\alpha_X[X]/100$ (seeble 2) for different rock types ordered according to Ti (and also Fe) concentrations.

Figure 1. Galactic cosmic ray (GCR) spectrum for a quiet and an active Sun [*Castagnoli and Lal*, 1980; *Reedy*, 1987b; *Masarik and Reedy*, 1994]. The bold curve is the averaged GCR flux on a solar cycle used in the simulations. The plotted flux is normalized by steradian and multiplied by a factor of 1.4 to take GCR alpha particles into account.

Figure 2. Bold curve: fast neutron leakage flux from uniform lunar soil of ferroan anorthosite (FAN) simulated between 500 keV and 10 MeV. Dotted curve: power law fit of the flux between 3 MeV and 10 MeV. Thin curve: total cross section of the oxygen-neutron interactions (ENDF/B-VI library).

Figure 3. Illustration of the Fe effect on the general shape of the simulated lunar neutron leakage flux. Energy bands correspond with Lunar Prospector fast neutron spectrometer ones. The bold curve represents the case without Fe. The thin curve is the case with 30% of Fe in the soil (in weight).

Figure 4. Spectrum of fast neutron leakage flux measured by Lunar Prospector over the Moon (Maurice et al., submitted manuscript, 1999). Asterisks represent the flux simulated for a soil of FAN and an averaged solar activity (this work).

Figure 5. Variation in integrated (500 keV to 8 MeV) value of fast neutron leakage flux from a soil of FAN with the abundance (weight percent) of Na, Mg, Al, Si, Ca, Ti, and Fe. Asterisks are simulation results ; the lines are linear fits. In each panel the initial composition of FAN is indicated by a vertical line.

Figure 6. Initial energy spectra of the produced neutrons per GCR particle in a FAN soil (solid curves) and in a pure iron soil (dashed curves). The thin curves represent the neutrons directly produced by primary GCR particles (i). The bold curves correspond to the total number of created neutrons (ii). Values are normalized by MeV.

Figure 7. Neutron leakage flux spectrum from a FAN soil compared to the total neutron production in the soil between 10 keV and 10 MeV. The leakage spectrum represents the number of neutrons per second and per MeV leaking out when 1 cm^2 of the surface is irradiated by an averaged GCR flux. The production spectrum represents the number of neutrons created in the soil per second and per MeV when 1 cm^2 of the surface is irradiated by an average GCR flux.

Figure 8. Variation of the simulated integrated values of fast neutron leakage flux for typical lunar rocks (triangles), (see Table 3) relative to their abundance of Fe and Ti. In Figure 8b the dashed line is a linear fit for typical lunar rocks. For comparison, the dotted lines represent the linear best fit of the relationship defined in Figure 5 for the modified FAN compositions.

Figure 9. Comparison of the integrated fluxes of fast neutrons as determined by the full numerical simulation (triangles) with the equivalent values calculated using the expression $J={}_X\Sigma\alpha_X[X]/100$ (seeble 2) for different rock types ordered according to Ti (and also Fe) concentrations.

Table 1. Ferroan Anorthosite Elemental Composition

	A	Z	n-p	W(weight fraction)	Oxide form	Woxide
O	15.999	8	0	0.456	-	-
Na	22.990	11	1	0.004	Na2O	0.006
Mg	24.305	12	0	0.005	MgO	0.008
Al	26.982	13	1	0.176	Al2O3	0.333
Si	28.086	14	0	0.207	SiO2	0.442
Ca	40.078	20	0	0.136	CaO	0.190
Ti	47.880	22	4	0.001	TiO2	0.001
Fe	55.847	26	4	0.015	FeO	0.019
			Total :	1	Total :	1

Composition used in the simulations. Abundance of each atom will be changed one by one to study effects on fast neutron flux. For example, if [Na] is set equal to 0, then [Na2O]=0 and the other oxide abundances are changed to keep a total of 1 while maintaining the same proportions between them.

Table 2. Coefficients for the Calculation of the Integrated Flux of Fast Neutron With a Linear Combination of Weight Fractions

	α^*
O	0.165
Na	1.28
Mg	1.68
Al	2.09
Si	2.26
Ca	1.75
Ti	3.02
Fe	2.81

*Units: neutron cm^{-2} s^{-1} weight $fraction^{-1}$.

Table 3. Typical Lunar Rock Compositions in Weight Fractions

	NOR	LM	KBN	Ap12	Ap11	Ap17
O	0.454	0.449	0.442	0.418	0.423	0.411
Na	0.004	0.003	0.006	0.002	0.003	0.003
Mg	0.065	0.040	0.035	0.054	0.046	0.060
Al	0.110	0.136	0.080	0.051	0.070	0.046
Si	0.229	0.213	0.250	0.213	0.199	0.180
S	-	-	-	-	0.001	-
K	0.002	0.0002	0.010	0.00005	0.001	0.0004
Ca	0.094	0.107	0.065	0.076	0.085	0.074
Ti	0.001	0.002	0.010	0.023	0.046	0.078
Cr	0.002	0.001	0.003	0.003	0.002	0.003
Mn	0.001	0.001	0.002	0.002	0.0016	0.002
Fe	0.038	0.046	0.085	0.159	0.122	0.142

From *Metzger and Drake* [1990]; *Feldman et al.* [1991]; *Phillips* [1986]. NOR, Norite; LM, Average Lunar Meteorite; KBN, KREEP; Ap12, Apollo 12 (low Ti); Ap11, Apollo 11; Ap17, Apollo 17 (high Ti).

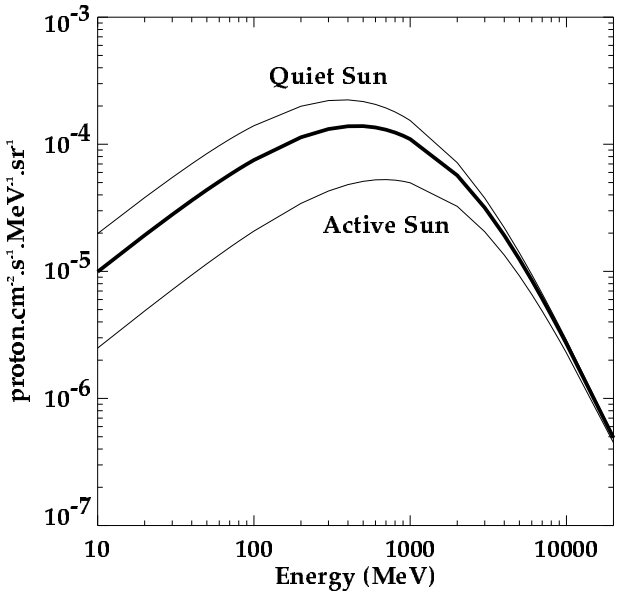

Figure 1. Galactic cosmic ray (GCR) spectrum for a quiet and an active Sun [Castagnoli and Lal, 1980; Reedy, 1987b; Masarik and Reedy, 1994]. The bold curve is the averaged GCR flux on a solar cycle used in the simulations. The plotted flux is normalized by steradian and multiplied by a factor of 1.4 to take GCR alpha particles into account.

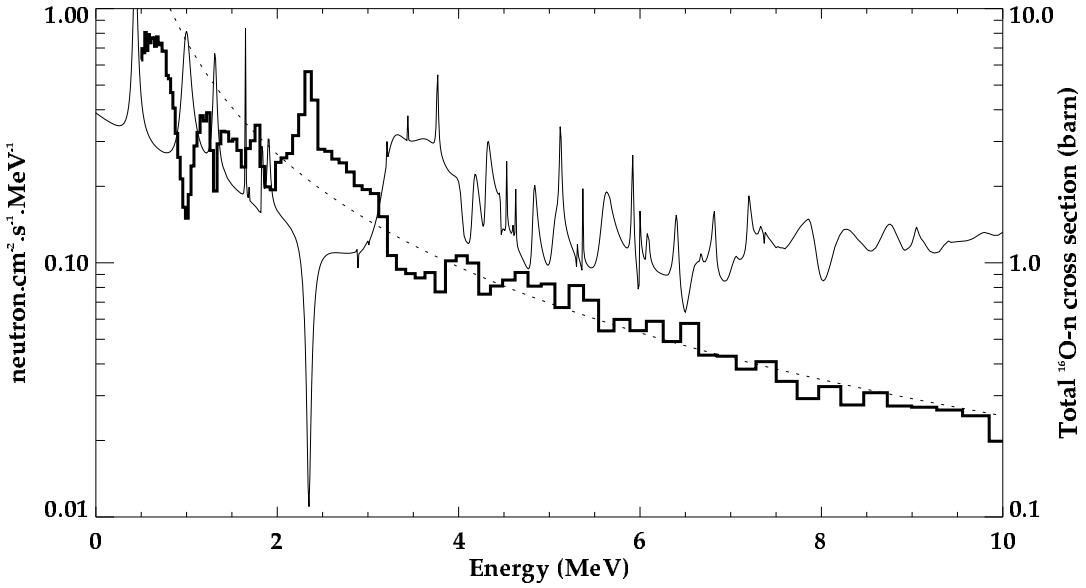

Figure 2. Bold curve: fast neutron leakage flux from uniform lunar soil of ferroan anorthosite (FAN) simulated between 500 keV and 10 MeV. Dotted curve: power law fit of the flux between 3 MeV and 10 MeV. Thin curve: total cross section of the oxygen-neutron interactions (ENDF/B-VI library).

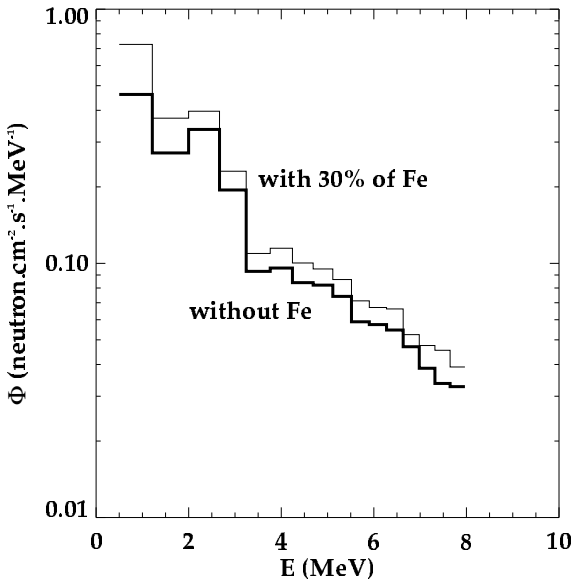

Figure 3. Illustration of the Fe effect on the general shape of the simulated lunar neutron leakage flux. Energy bands correspond with LUNAR PROSPECTOR fast neutron spectrometer ones. The bold curve represents the case without Fe. The thin curve is the case with 30% of Fe in the soil (in weight).

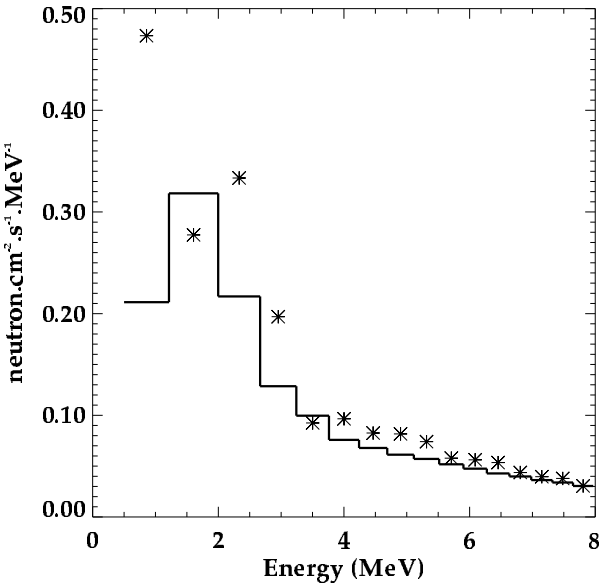

Figure 4. Spectrum of fast neutron leakage flux measured by LUNAR PROSPECTOR over the Moon (Maurice et al., submitted manuscript, 1999). Asterisks represent the flux simulated for a soil of FAN and an averaged solar activity (this work).

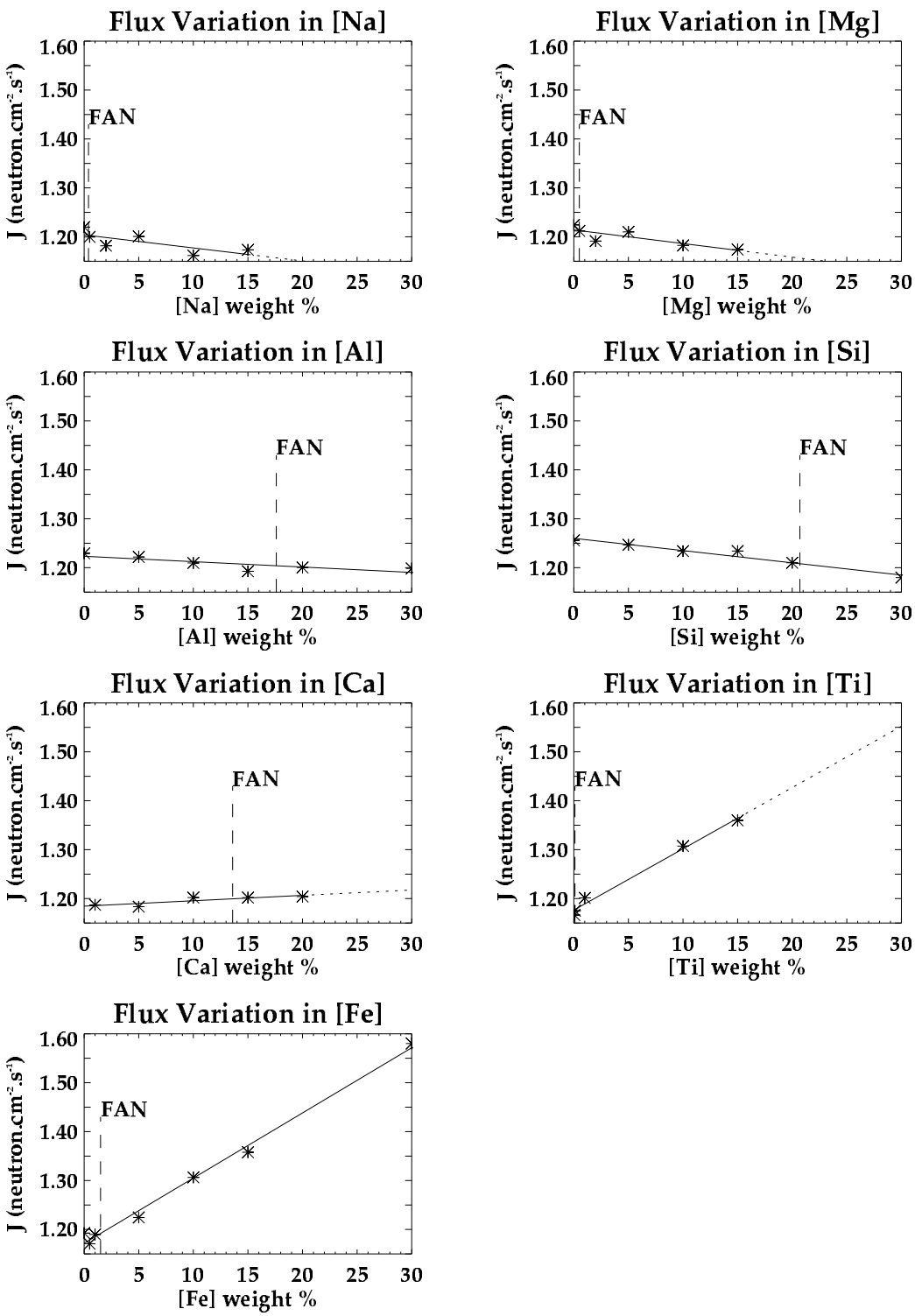

Figure 5. Variation in integrated (500 keV to 8 MeV) value of fast neutron leakage flux from a soil of FAN with the abundance (weight percent) of Na, Mg, Al, Si, Ca, Ti, and Fe. Asterisks are simulation results ; the lines are linear fits. In each panel the initial composition of FAN is indicated by a vertical line.

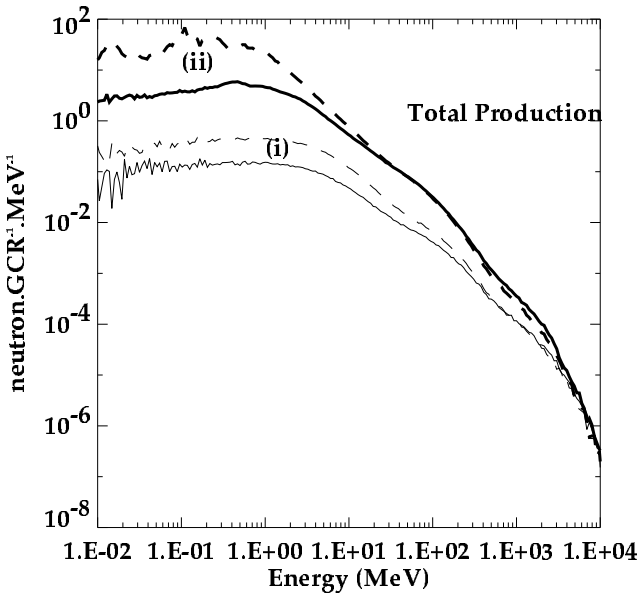

Figure 6. Initial energy spectra of the produced neutrons per GCR particle in a FAN soil (solid curves) and in a pure iron soil (dashed curves). The thin curves represent the neutrons directly produced by primary GCR particles (i). The bold curves correspond to the total number of created neutrons (ii). Values are normalized by MeV.

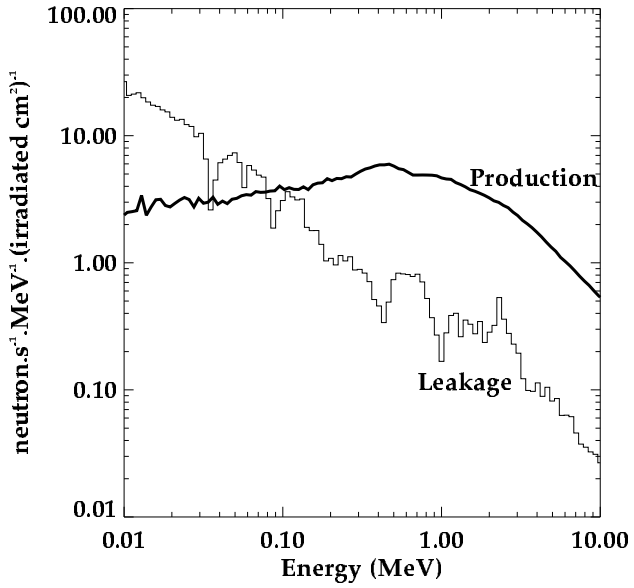

Figure 7. Neutron leakage flux spectrum from a FAN soil compared to the total neutron production in the soil between 10 keV and 10 MeV. The leakage spectrum represents the number of neutrons per second and per MeV leaking out when 1 cm2 of the surface is irradiated by an averaged GCR flux. The production spectrum represents the number of neutrons created in the soil per second and per MeV when 1 cm2 of the surface is irradiated by an average GCR flux.

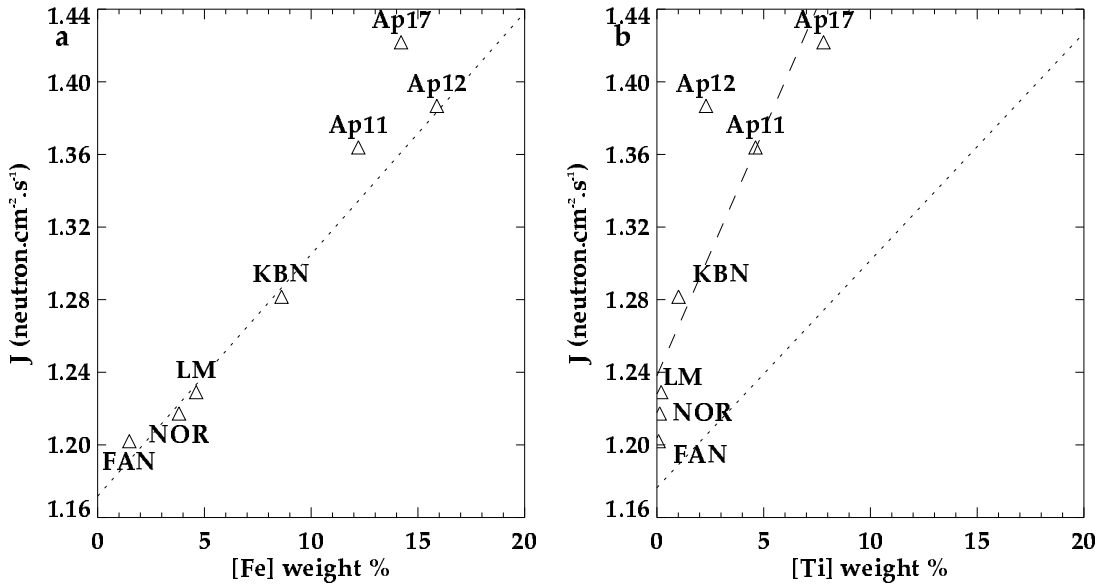

Figure 8. Variation of the simulated integrated values of fast neutron leakage flux for typical lunar rocks (triangles), (see Table 3) relative to their abundance of Fe and Ti. In Figure8b the dashed line is a linear fit for typical lunar rocks. For comparison, the dotted lines represent the linear best fit of the relationship defined in Figure 5 for the modified FAN compositions.

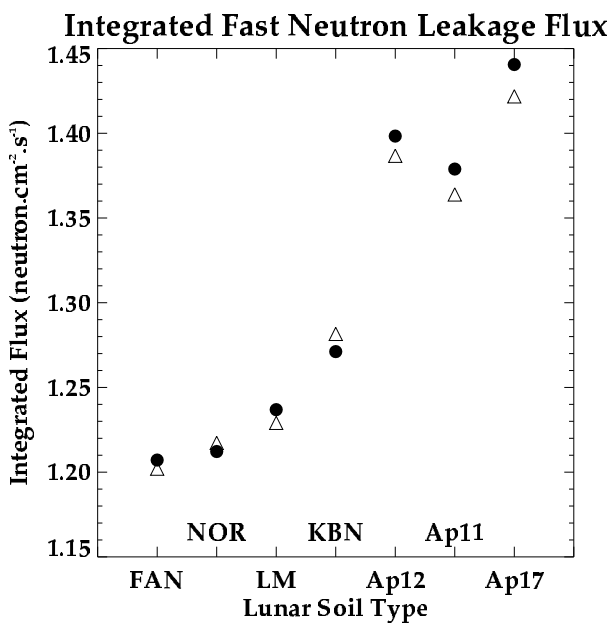

Figure 9. Comparison of the integrated fluxes of fast neutrons as determined by the full numerical simulation (triangles) with the equivalent values calculated using the expression $J={}_X\Sigma\alpha_X[X]/100$ (see Table 2) for different rock types ordered according to Ti (and also Fe) concentrations.